Available online at www.sciencedirect.com
SCIENCE DIRECT
Journal of Sound and Vibration 295 (2006) 479–490
JOURNAL OF SOUND AND VIBRATION
www.elsevier.com/locate/jsvi

Longitudinal wave propagation. Part II—Analysis of crack influence

Marek Krawczuk[a,b,*], Joanna Grabowska[a], Magdalena Palacz[a]

[a]*Institute of Fluid Flow Machinery, PAS, Fiszera 14, 80–952 Gdańsk, Poland*
[b]*Department of Electrical Engineering and Automatic, Technical University of Gdansk, Narutowicza 11/12, 80–952 Gdańsk, Poland*

Received 5 January 2004; received in revised form 14 November 2005; accepted 19 December 2005
Available online 23 March 2006

Abstract

The aim of this paper is to introduce new spectral finite elements for damage detection in cracked rods. The four new spectral elements are based on the elementary, Love, Mindlin–Herrmann, and three-mode theories of rods. For all the models the crack is substituted by means of a dimensionless spring. Numerical examples show the influence of a fatigue, non-propagating, open crack on wave propagation in rods. For the models analysed differences in behaviour of the longitudinal waves are observed. The differences between signals reflected from the crack in the proposed models are functions of the excitation signal frequency.

1. Introduction

Structural health monitoring and damage detection has received a considerable amount of attention over the last few decades. Previous approaches to non-destructive evaluation of structures, and assessing their integrity, typically involved some form of human interaction. Recent advances in smart materials technology have resulted in a renewed interest in developing advanced self-diagnostic methods for assessing the state of a structure without any human interaction [1–3]. The goal is to reduce the human interaction while monitoring the integrity of a structure. With this goal in mind, many researchers have made significant progress in developing damage detection methods for structures based on traditional modal analysis techniques [4–9]. These techniques are often well suited for the detection of rather significant defects because small defects do not influence changes in the lower frequencies, thus global behavior of the system is not affected. For this reason new methods based on smart materials have been rapidly developed in last years.

New damage detection methods are based on analysing anomalies in elastic wave propagation in structures [10–14]. Damage detection systems utilise the well-known fact that material discontinuities affect elastic waves propagating in solids. Wave frequencies that are most sensitive to damage depend on the type of structure, the material, and the form of damage. Elastic waves are generated and sensed by an array of transducers either embedded in, or bonded to, the surface of a structure.

*Corresponding author. Institute of Fluid Flow Machinery, Polish Academy of Sciences, Fiszera 14, 80–952 Gdańsk, Poland. Tel.: +48 58 341 12 71 x 206; fax: +48 58 341 44 61.
E-mail address: mk@imp.gda.pl (M. Krawczuk).

0022-460X/$ - see front matter © 2006 Elsevier Ltd. All rights reserved.
doi:10.1016/j.jsv.2005.12.049

The main objective of the theoretical portion of this problem is to develop a model that can determine the relationship between the power of a transducer, the frequency of a generated signal, the type of monitored solid, and the range of effective signal transmission. The frequencies used in this technique are much higher than those typically used in modal analysis based methods, but lower than in ultrasonic testing. At such high frequencies, the responses are dominated by local modes and at the same time the wavelength of the excitation is small enough to detect incipient-type damage.

Problems of longitudinal wave propagation in cracked rods have until now been studied using elementary rod theory which assumes a constant longitudinal displacement along the cross-section of a rod, and also neglects any transverse deflection [15,16]. The real deformation of the rod is more complicated, and in broad terms three distinct behaviours can be identified. The first is that the longitudinal displacement has a non-zero mean value, the second is that the transverse deflection is nearly linear, and the third is that the longitudinal displacement has an almost parabolic distribution. It means that higher order rod theories should have two additional deformation modes—the transverse deflection and the parabolic longitudinal displacement along the rod.

For developing the spectral elements with cracks the approach presented in Ref. [19] is used. In all cases the crack is substituted by a dimensionless spring of flexibility θ and is modelled by Castigliano's theorem and the laws of fracture mechanics [17]. Using the proposed spectral element with the crack allows one to analyse high frequency excitation signals for low computational times, and with high numerical accuracy. Applying the spectral element with the crack also allows the element stiffness and mass distribution to be modelled in a better and more exact way in comparison with treating the crack as a boundary in itself. The facts mentioned above are undoubtedly important features and may have a big influence on modern damage monitoring techniques.

A procedure for creating the dynamic stiffness matrix for all the models is described in detail. Numerical examples illustrate the wave propagation process in cracked rods for all the models developed. Results from numerical calculations show considerable differences in the behaviour of longitudinal waves in cracked rods for the modified rod theories. The above differences are a function of the frequency of the excitation signal.

2. Spectral elements for cracked rods

The spectral finite elements developed for a rod with a transverse open and non-propagating crack are based on the theories presented in Ref. [19], and are given in Fig. 1. The elements are of length L and the cross-sectional area is equal to A. The crack is replaced by a dimensionless spring with flexibility θ, which is calculated by using Castigliano's theorem and laws of fracture mechanics. A detailed description is given next in Section 2.1.

2.1. Flexibility at the crack location

The flexibility at the crack location for the spectral rod elements can be represented by means of Castigliano's theorem:

$$c_{ij} = \frac{\partial^2 U}{\partial S_i \partial S_j} \quad (\text{for } i = j = 1), \tag{1}$$

where U denotes the elastic strain energy of the element caused by the presence of the crack and the S values are independent nodal forces acting on the element.

The following relation can express the elastic strain energy due to the appearance of the crack,

$$U = \frac{1}{E}\int_A K_I^2 \, \mathrm{d}A, \tag{2}$$

where A denotes the area of the crack and K_I is a stress intensity factor corresponding to the first mode of the crack formation [18].

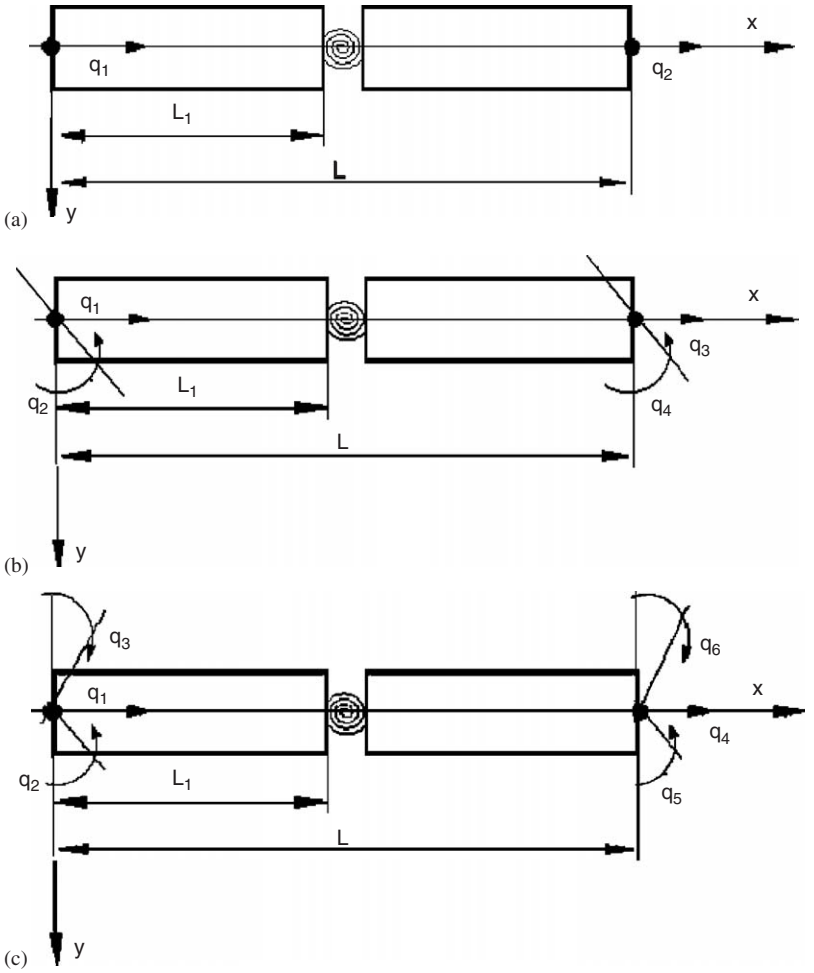

Fig. 1. Cracked spectral element models for the elementary and Love rod theories (a), for the Mindlin–Herrmann rod theory (b) and for the three-mode rod theory (c).

The stress intensity factor can be expressed as follows:

$$K_I = \frac{S_1}{A}\sqrt{\pi\alpha} f\left(\frac{\alpha}{h}\right), \tag{3}$$

where α and h are defined in Fig. 2, and f is a correction function in the form as given by [18]

$$f\left(\frac{\alpha}{h}\right) = \sqrt{\frac{\tan(\pi\alpha/2h)}{\pi\alpha/2h}}\left[\frac{0.752 + 2.02(\alpha/h) + 0.37[1 - \sin(\pi\alpha/2h)]^3}{\cos(\pi\alpha/2h)}\right]. \tag{4}$$

After simple transformations the flexibility of the elastic element modelling the cracked cross section of the spectral rod finite element can be rewritten as

$$c = \frac{2}{Eb}\int_0^{\bar{a}} \bar{\alpha} f^2(\bar{\alpha})\, \mathrm{d}\bar{a}, \tag{5}$$

where $\bar{a} = \alpha/h$, $\bar{\alpha} = \alpha/h$, with the details given in Fig. 2.

In non-dimensional form the flexibility c can be expressed as

$$\theta = EAc. \tag{6}$$

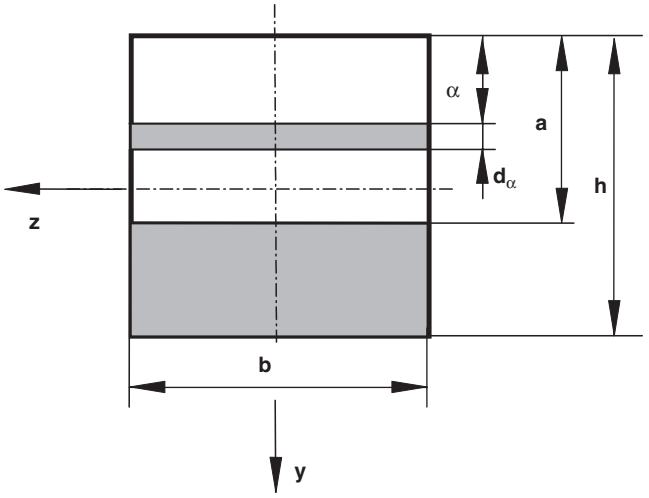

Fig. 2. Cross section of the rod at the crack location.

2.2. Spectral rod element based on elementary and Love theories

A spectral rod element based on elementary rod theory has been developed by Palacz and Krawczuk [16] and the spectral element for a cracked rod based on Love rod theory is shown in Fig. 1a. The element has two nodes and one degree of freedom per node. The longitudinal displacement u_0 can be expressed for the left and right part of the element as follows:

$$\hat{u}_{0,1}(x) = A_1 e^{-ikx} + B_1 e^{-ik(L_1-x)} \quad \text{for } x \in (0, L_1), \tag{7}$$

$$\hat{u}_{0,2}(x) = A_2 e^{-ik(L_1+x)} + B_2 e^{-ik[L-(L_1+x)]} \quad \text{for } x \in (0, L-L_1) \tag{8}$$

where k is the wavenumber stated in Eq. (7) in Ref. [19].

The constants A_1, B_1, A_2 and B_2 can be found using the following boundary conditions:

- for the left end of the element ($x = 0$):

$$\hat{u}_{0,1}(x) = \hat{q}_1, \tag{9}$$

- at the crack location ($x = L_1$ for $\hat{u}_{0,1}(x)$ and $x = 0$ for $\hat{u}_{0,2}(x)$):

$$\hat{u}_{0,2}(x) - \hat{u}_{0,1}(x) = \theta \frac{\partial \hat{u}_{0,1}(x)}{\partial x}, \tag{10}$$

$$\frac{\partial \hat{u}_{0,1}(x)}{\partial x} = \frac{\partial \hat{u}_{0,2}(x)}{\partial x}, \tag{11}$$

- for the right end of the element ($x = L–L_1$):

$$\hat{u}_{0,2}(x) = \hat{q}_2, \tag{12}$$

where q_1, q_2 denotes nodal axial displacements.

Taking Eqs. (7) and (8) into account and the boundary conditions given by Eqs. (9)–(12) the constants A_1, B_1, A_2 and B_2 can be expressed as functions of the nodal displacements in the following manner:

$$\begin{bmatrix} A_1 \\ B_1 \\ A_2 \\ B_2 \end{bmatrix} = W^{-1} \begin{bmatrix} \hat{q}_1 \\ 0 \\ 0 \\ \hat{q}_2 \end{bmatrix}, \tag{13}$$

where

$$W = \begin{bmatrix} 1 & e^{-ikL_1} & 0 & 0 \\ (-1+ik\theta)e^{-ikL_1} & (-1-ik\theta) & e^{-ikL_1} & e^{-ik(L-L_1)} \\ -ike^{-ikL_1} & ik & ike^{-ikL_1} & -ike^{-ik(L-L_1)} \\ 0 & 0 & e^{-ikL} & 1 \end{bmatrix}. \tag{14}$$

Nodal forces are given by the following expressions:

- for the left end of the element ($x = 0$):

$$\hat{F}_1 = EA\frac{\partial \hat{u}_{0,1}(x)}{\partial x} - v^2\rho J\omega^2 \frac{\partial \hat{u}_{0,1}(x)}{\partial x}, \tag{15}$$

- for the right end of the element ($x = L - L_1$):

$$\hat{F}_2 = EA\frac{\partial \hat{u}_{0,2}(x)}{\partial x} - v^2\rho J\omega^2 \frac{\partial \hat{u}_{0,2}(x)}{\partial x}. \tag{16}$$

The relationship between the nodal forces and the nodal displacements denotes the dynamic stiffness matrix $\mathbf{K}_{\mathrm{dyn}}$ of the spectral element for the cracked rod, and is given by

$$\begin{bmatrix} \hat{F}_1 \\ \hat{F}_2 \end{bmatrix} = \mathbf{K}_{\mathrm{dyn}} \begin{bmatrix} \hat{q}_1 \\ \hat{q}_2 \end{bmatrix}, \tag{17}$$

with

$$\mathbf{K}_{\mathrm{dyn}} = (EA - v^2\rho J\omega^2) \begin{bmatrix} ik & -ike^{-ikL_1} & 0 & 0 \\ 0 & 0 & -ike^{-ikL} & ik \end{bmatrix} W^{-1}. \tag{18}$$

2.3. Spectral rod element based on Mindlin–Herrmann theory

The spectral element for a cracked rod based on Mindlin–Herrmann rod theory is presented in Fig. 1b. The element has two nodes and two degrees of freedom per node. The longitudinal displacement u_0 and rotation ψ_0 can be expressed for the left and right part of the element as follows:

$$\begin{aligned} \hat{u}_{0,1} &= A_1R_1e^{-ik_1x} + B_1R_2e^{-ik_2x} - C_1R_1e^{-ik_1(L_1-x)} - D_1R_2e^{-ik_2(L_1-x)} && \text{for } x \in (0, L_1), \\ \hat{\psi}_{0,1} &= A_1e^{-ik_1x} + B_1e^{-ik_2x} + C_1e^{-ik_1(L_1-x)} + D_1e^{-ik_2(L_1-x)} && \text{for } x \in (0, L_1), \\ \hat{u}_{0,2} &= A_2R_1e^{-ik_1(L_1+x)} + B_2R_2e^{-ik_2(L_1+x)} - C_2R_1e^{-ik_1(L-(L_1+x))} \\ &\quad - D_2R_2e^{-ik_2(L-(L_1+x))} && \text{for } x \in (L_1, L-L_1), \\ \hat{\psi}_{0,2} &= A_1e^{-ik_1(L_1+x)} + B_2e^{-ik_2(L_1+x)} + C_2e^{-ik_1(L-(L_1+x))} + D_2e^{-ik_2(L-(L_1+x))} && \text{for } x \in (L_1, L-L_1), \end{aligned} \tag{19}$$

with

$$R_i = \frac{\mathrm{i}k_i\lambda A}{-(2\mu+\lambda)Ak_i^2 + \rho A\omega^2}, \quad i = 1,2, \tag{20}$$

where k_1 and k_2 denote the wavenumbers, which are a solution of Eq. (24) from Ref. [19].

In order to calculate unknown constants A_1, B_1, C_1, D_1, A_2, B_2, C_2 and D_2 the following boundary conditions are used:

- for the left end of the element ($x = 0$):

$$\hat{u}_{0,1}(x) = \hat{q}_1, \quad \hat{\psi}_{0,1}(x) = \hat{q}_2, \tag{21}$$

- at the crack location ($x = L_1$ for $\hat{u}_{0,1}(x)$, $\hat{\psi}_{0,1}(x)$ and $x = 0$ for $\hat{u}_{0,2}(x)$, $\hat{\psi}_{0,2}(x)$):

$$\hat{u}_{0,2}(x) - \hat{u}_{0,1}(x) = \theta^* \frac{\partial \hat{u}_{0,1}(x)}{\partial x} + \lambda\hat{\psi}_{0,1}(x), \tag{22}$$

$$(2\mu+\lambda)A\frac{\partial \hat{u}_{0,1}(x)}{\partial x} + \lambda A\hat{\psi}_{0,1}(x) = (2\mu+\lambda)A\frac{\partial \hat{u}_{0,2}(x)}{\partial x} + \lambda A\hat{\psi}_{0,2}(x), \tag{23}$$

$$\hat{\psi}_{0,1}(x) = \hat{\psi}_{0,2}(x), \tag{24}$$

$$\frac{\partial \hat{\psi}_{0,1}(x)}{\partial x} = \frac{\partial \hat{\psi}_{0,2}(x)}{\partial x}, \tag{25}$$

- for the right end of the element ($x = L–L_1$):

$$\hat{u}_{0,2}(x) = \hat{q}_3, \quad \hat{\psi}_{0,2}(x) = \hat{q}_4, \tag{26}$$

where $\hat{q}_1, \hat{q}_3$ denote the nodal axial displacements, $\hat{q}_2, \hat{q}_4$ are the nodal rotations, and $\theta^* = c(2\mu+\lambda)A$.

Applying Eq. (19) and the boundary conditions given by Eqs. (21)–(26) the constants A_1, B_1, C_1, D_1, A_2, B_2, C_2 and D_2 can be expressed as functions of the nodal displacements.

The nodal forces are given by the following formulas:

- for the left end of the element ($x = 0$):

$$\begin{aligned} \hat{F}_1 &= (2\mu+\lambda)A\frac{\partial \hat{u}_{0,1}(x)}{\partial x} + \lambda A\hat{\psi}_{0,1}(x), \\ \hat{F}_2 &= \mu I K_1\left(\frac{\partial \hat{\psi}_{0,1}(x)}{\partial x}\right), \end{aligned} \tag{27}$$

- for the right end of the element ($x = L–L_1$):

$$\begin{aligned} \hat{F}_3 &= (2\mu+\lambda)A\frac{\partial \hat{u}_{0,2}(x)}{\partial x} + \lambda A\hat{\psi}_{0,2}(x), \\ \hat{F}_4 &= \mu I K_1\left(\frac{\partial \hat{\psi}_{0,2}(x)}{\partial x}\right). \end{aligned} \tag{28}$$

Then using the expressions for calculating constants A_1, B_1, C_1, D_1, A_2, B_2, C_2 and D_2 as functions of the nodal displacements, the relation between the nodal forces and the nodal displacements can be obtained. The

square, symmetric matrix in this relation denotes the dynamic stiffness matrix $\mathbf{K}_{\mathrm{dyn}}$ of the cracked spectral element based on the Mindlin–Herrmann rod theory.

2.4. Spectral elements based on three-mode rod theory

The spectral element for a cracked rod based on three-mode rod theory is given in Fig. 1c. The element has two nodes and three degrees of freedom per node. The longitudinal displacement $\hat{u}_0$ and rotations $\hat{\psi}_0$, $\hat{\phi}_0$ can be expressed for the left and right part of the element as follows:

$$\begin{aligned}
\hat{u}_{0,1} &= A_1R_4\mathrm{e}^{-\mathrm{i}k_1x} + B_1R_5\mathrm{e}^{-\mathrm{i}k_2x} + C_1R_6\mathrm{e}^{-\mathrm{i}k_3x} + D_1R_4\mathrm{e}^{-\mathrm{i}k_1(L_1-x)} \\
&\quad + E_1R_5\mathrm{e}^{-\mathrm{i}k_2(L_1-x)} + F_1R_6\mathrm{e}^{-\mathrm{i}k_3(L_1-x)}, \\
\hat{\psi}_{0,1} &= A_1R_1\mathrm{e}^{-\mathrm{i}k_1x} + B_1R_2\mathrm{e}^{-\mathrm{i}k_2x} + C_1R_3\mathrm{e}^{-\mathrm{i}k_3x} - D_1R_1\mathrm{e}^{-\mathrm{i}k_1(L_1-x)} \\
&\quad - E_1R_2\mathrm{e}^{-\mathrm{i}k_2(L_1-x)} - F_1R_3\mathrm{e}^{-\mathrm{i}k_3(L_1-x)}, \\
\hat{\phi}_{0,1} &= A_1\mathrm{e}^{-\mathrm{i}k_1x} + B_1\mathrm{e}^{-\mathrm{i}k_2x} + C_1\mathrm{e}^{-\mathrm{i}k_3x} + D_1\mathrm{e}^{-\mathrm{i}k_1(L_1-x)} \\
&\quad + E_1\mathrm{e}^{-\mathrm{i}k_2(L_1-x)} + F_1\mathrm{e}^{-\mathrm{i}k_3(L_1-x)}, \\
\hat{u}_{0,2} &= A_2R_4\mathrm{e}^{-\mathrm{i}k_1(L_1+x)} + B_2R_5\mathrm{e}^{-\mathrm{i}k_2(L_1+x)} + C_2R_6\mathrm{e}^{-\mathrm{i}k_3(L_1+x)} + D_2R_4\mathrm{e}^{-\mathrm{i}k_1(L-(L_1+x))} \\
&\quad + E_2R_5\mathrm{e}^{-\mathrm{i}k_2(L-(L_1+x))} + F_2R_6\mathrm{e}^{-\mathrm{i}k_3(L-(L_1+x))}, \\
\hat{\psi}_{0,2} &= A_2R_1\mathrm{e}^{-\mathrm{i}k_1(L_1+x)} + B_2R_2\mathrm{e}^{-\mathrm{i}k_2(L_1+x)} + C_2R_3\mathrm{e}^{-\mathrm{i}k_3(L_1+x)} - D_2R_1\mathrm{e}^{-\mathrm{i}k_1(L-(L_1+x))} \\
&\quad - E_2R_2\mathrm{e}^{-\mathrm{i}k_2(L-(L_1+x))} - F_2R_3\mathrm{e}^{-\mathrm{i}k_3(L-(L_1+x))}, \\
\hat{\phi}_{0,2} &= A_2\mathrm{e}^{-\mathrm{i}k_1(L_1+x)} + B_2\mathrm{e}^{-\mathrm{i}k_2(L_1+x)} + C_2\mathrm{e}^{-\mathrm{i}k_3(L_1+x)} + D_2\mathrm{e}^{-\mathrm{i}k_1(L-(L_1+x))} \\
&\quad + E_2\mathrm{e}^{-\mathrm{i}k_2(L-(L_1+x))} + F_2\mathrm{e}^{-\mathrm{i}k_3(L-(L_1+x))},
\end{aligned} \tag{29}$$

with

$$\begin{aligned}
R_i &= -\frac{(2\mu+\lambda)Ik_i^2 + 5\mu A - \rho I\omega^2}{0.2083\,\mathrm{i}\mu Ah}, \quad \mathrm{i} = 1,2,3, \\
R_i &= -\frac{\mathrm{i}k_j\lambda A}{(2\mu+\lambda)Ak_j^2 + \rho A\omega^2}R_j, \quad \mathrm{i} = 4,5,6, \quad j = 1,2,3,
\end{aligned} \tag{30}$$

where k_1, k_2 and k_3 denote the wave numbers which are a solution of Eq. (38) in Ref. [19].

In order to calculate the constants A_1, B_1, C_1, D_1, E_1, F_1, A_2, B_2, C_2, D_2, E_2 and F_2 the following boundary conditions are used,

- for the left end of the element ($x = 0$):

$$\hat{u}_{0,1}(x) = q_1, \quad \hat{\psi}_{0,1}(x) = q_2, \quad \hat{\phi}_{0,1}(x) = q_3, \tag{31}$$

- at the crack location ($x = L_1$ for $\hat{u}_{0,1}(x)$, $\hat{\psi}_{0,1}(x)$, $\hat{\phi}_{0,1}(x)$ and $x = 0$ for $\hat{u}_{0,2}(x)$, $\hat{\psi}_{0,2}(x)$, $\hat{\phi}_{0,2}(x)$):

$$\hat{u}_{0,2}(x) - \hat{u}_{0,1}(x) = \theta^* \frac{\partial \hat{u}_{0,1}(x)}{\partial x} + \lambda\hat{\psi}_{0,1}(x), \tag{32}$$

$$(2\mu+\lambda)A\frac{\partial \hat{u}_{0,1}(x)}{\partial x} + \lambda A\hat{\psi}_{0,1}(x) = (2\mu+\lambda)A\frac{\partial \hat{u}_{0,2}(x)}{\partial x} + \lambda A\hat{\psi}_{0,2}(x), \tag{33}$$

$$\hat{\psi}_{0,1}(x) = \hat{\psi}_{0,2}(x), \tag{34}$$

$$\left(\frac{\partial\hat{\psi}_{0,1}(x)}{\partial x}-24\frac{\hat{\phi}_{0,1}(x)}{h}\right)=\left(\frac{\partial\hat{\psi}_{0,2}(x)}{\partial x}-24\frac{\hat{\phi}_{0,2}(x)}{h}\right), \tag{35}$$

$$\hat{\phi}_{0,1}(x)=\hat{\phi}_{0,2}(x), \tag{36}$$

$$\frac{\partial\hat{\phi}_{0,1}(x)}{\partial x}=\frac{\partial\hat{\phi}_{0,2}(x)}{\partial x}, \tag{37}$$

- for the right end of the element ($x = L–L_1$):

$$\hat{u}_{0,2}(x)=\hat{q}_4,\quad \hat{\psi}_{0,2}(x)=\hat{q}_5,\quad \hat{\phi}_{0,2}(x)=\hat{q}_6, \tag{38}$$

where $\hat{q}_1,\hat{q}_4$ denote the nodal axial displacements, $\hat{q}_2,\hat{q}_3,\hat{q}_5,\hat{q}_6$ are the nodal rotations, and $\theta^*=c(2\mu+\lambda)A$.Eq. (29), and the boundary conditions given by Eqs. (31)–(38), can be used to derive the constants A_1, B_1, C_1, D_1, E_1, F_1, A_2, B_2, C_2, D_2, E_2 and F_2 , which can be expressed as functions of the nodal displacements.

The nodal forces are given by the following:

- for the left end of the element ($x = 0$):

$$\begin{aligned}\hat{F}_1&=(2\mu+\lambda)A\frac{\partial\hat{u}_{0,1}(x)}{\partial x}+\lambda A\hat{\psi}_{0,1}(x),\\ \hat{F}_2&=\mu I\left(\frac{\partial\hat{\psi}_{0,1}(x)}{\partial x}-24\frac{\hat{\phi}_{0,1}(x)}{h}\right),\\ \hat{F}_3&=\tfrac{48}{5}(2\mu+\lambda)I\frac{\partial\hat{\phi}_{0,1}(x)}{\partial x},\end{aligned} \tag{39}$$

- for the right end of the element ($x = L–L_1$):

$$\begin{aligned}\hat{F}_4&=(2\mu+\lambda)A\frac{\partial\hat{u}_{0,2}(x)}{\partial x}+\lambda A\hat{\psi}_{0,2}(x),\\ \hat{F}_5&=\mu I\left(\frac{\partial\hat{\psi}_{0,2}(x)}{\partial x}-24\frac{\hat{\phi}_{0,2}(x)}{h}\right),\\ \hat{F}_6&=\tfrac{48}{5}(2\mu+\lambda)I\frac{\partial\hat{\phi}_{0,2}(x)}{\partial x}.\end{aligned} \tag{40}$$

By using the equations for constructing the constants A_1, B_1, C_1, D_1, E_1, F_1, A_2, B_2, C_2, D_1, E_1 and F_2 as functions of the nodal displacements, the relation between the nodal forces and the nodal displacements can be calculated. The square, symmetric matrix in this relation denotes the dynamic stiffness matrix $\mathbf{K}_{\mathrm{dyn}}$ of the cracked spectral element based on the three-mode rod theory.

3. Numerical examples

The main idea of the numerical calculations is to observe how waves propagate in a cracked rod for the different rod theories discussed above. Results from the numerical calculations for the elementary, Love, Mindlin–Herrmann, and three-mode rod theories are presented and discussed below.

All the numerical calculations were carried out for a cantilever steel rod. The rod was modelled by one spectral element with a crack and one throw-off element (see Ref. [19] for details). The length of the rod is 4 m, the width 0.02 m and the breadth 0.02 m. The following material properties are utilised; Young's modulus

210 GPa, Poisson ratio 0.3 and density 7850 kg/m^3. In all the numerical examples the depth of the crack is equal to 20% of the rod breadth.

The analysis was carried out by exciting two out of three signals, as in Ref. [19]. Referring to that paper, the signal shapes in the time and frequency domains are given such that the (a) signal in Fig. 2 in the paper allows the excitation of vibration modes at around 80 kHz, whereas with the (b) signal vibration modes at around 160 kHz can be analysed. The results of the analysis in Ref. [19] clearly show that the (b) signal should excite all modes of vibration, for the theories that have been investigated.

This understanding is extended within Figs. 3–5 in this paper, and these present a comparison of the reflected signals obtained for the rod with a crack modelled by all of the theories discussed in this paper. For a better illustration of the differences in signals, the accelerations calculated for all the models were normalised according to their maximum value. In all cases the crack was located 2 m from the free end of the rod and responses were calculated at the free end. The first plot denoted by (a) in Fig. 3 illustrates the differences in the reflected signal obtained for elementary and Love rod theories excited with a lower frequency signal (refer to Fig. 2a in Ref. [19]) while the second one in Fig. 3b shows the differences achieved for the same theories but excited with a higher frequency signal (and refer to Fig. 2b in Ref. [19]). One can notice additional reflections that are not present in Figs. 7, 8, and 13 of Ref. [19]. These come from the crack location, where the signal divides into two parts; the first part reflects, and the second goes through the crack and reflects from the clamped end. It may be seen that the differences are functions of the excitation signal frequency. The higher the frequency is, the more reflections appear. Nevertheless the relative location of additional reflections from the crack position is the same for both the excitation signal cases that were analysed.

Fig. 4 summarises a comparison of results obtained for the elementary and Mindlin–Herrmann rod theories. The rod under analysis was excited with the same signals as used in Ref. [19]. The composition of the plots is similar to that of Fig. 3. The differences between the responses are bigger than for the Love model, especially for a higher frequency excitation signal. This is because the model based on the Mindlin–Herrmann theory takes two vibration modes of wave propagation into account. This conclusion may lead to a more optimal application by means of the Mindlin–Herrmann theory for the analysis of high frequency excitation signals, mainly because the result obtained for the rod modelled with that theory shows that the wave propagates faster. This is closer to the behaviour of real physical systems.

The last graphs presented here illustrate the differences between the responses obtained for the elementary and three-mode rod theories. The interpretation is the same as for Figs. 3 and 4. As may be seen on the graph of Fig. 5a, the responses obtained for the lower frequency signal for the elementary and three-mode theories

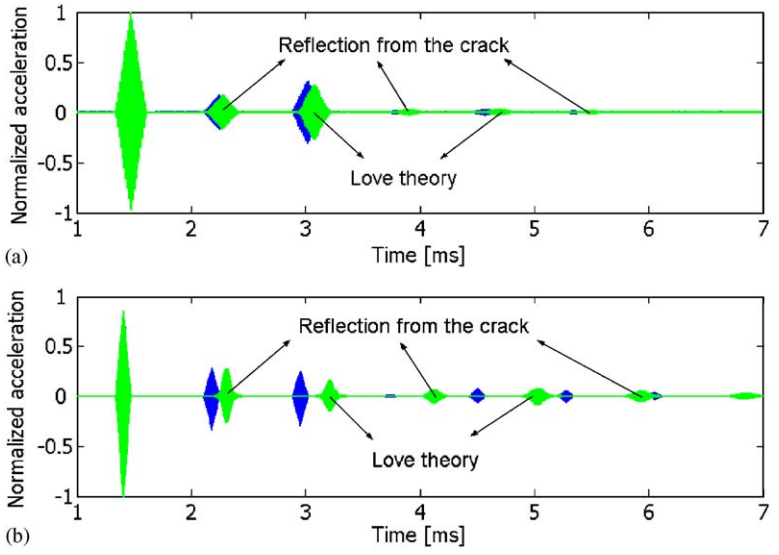

Fig. 3. Comparison of signals obtained for elementary and Love rod theories with lower frequency signal (a) and higher frequency signal (b).

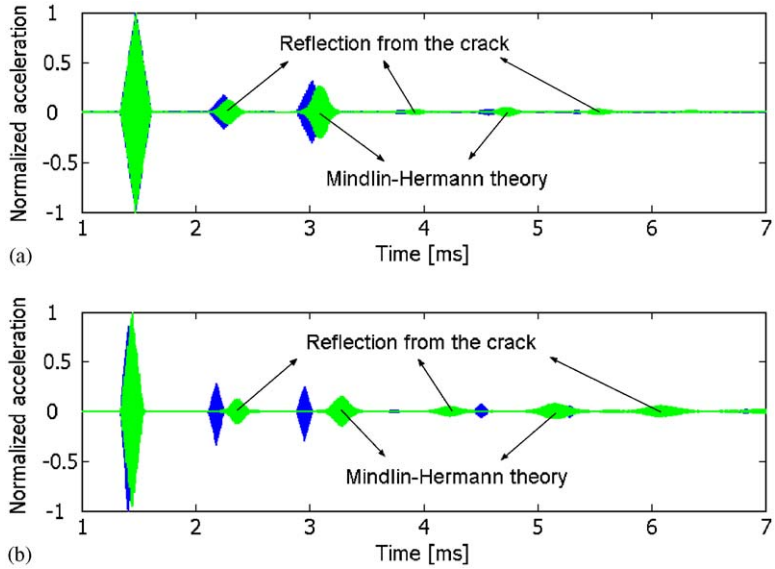

Fig. 4. Comparison of signals obtained for elementary and Mindlin–Herrmann rod theories with lower frequency signal (a) and higher frequency signal (b).

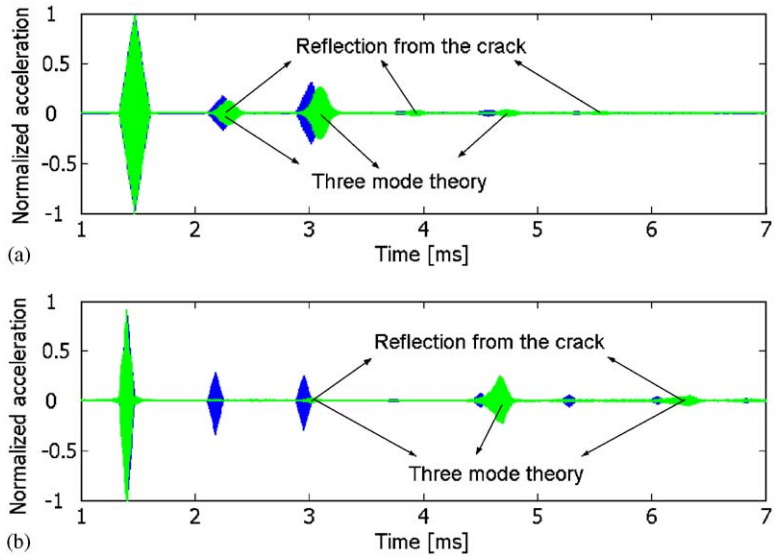

Fig. 5. Comparison of signals obtained for elementary and three-mode rod theories with lower frequency signal (a) and higher frequency signal (b).

do not differ significantly. On the other hand responses obtained for the higher frequency signal are definitely not similar. This happens due to the fact that the three-mode theory allows the consideration of three vibration modes. If the signal is of very high frequency, the numerical model for the analysis of such systems must be based on proper theory. It should take into account all of the modes of the propagating signal.

4. Conclusions

This paper presents new spectral elements for a rod with a non-propagating transverse open crack, and these elements can be utilised for effective wave propagation analysis. The novelty of the approach presented

here is associated with using several different rod theories for modelling the element; namely the Love, Mindlin–Herrmann and three-mode theories. For the analysis the spectral element method was utilised because this method allows the modelling of a real cracked rod with one element when the geometry is not affected. The procedure for calculating the dynamic stiffness matrix is developed for each theory respectively.

The paper presents a comparison of results obtained for two specific high frequency signals for each theory. The differences between the responses are significant with an increasing excitation signal frequency. It was shown that models based on the Mindlin–Herrmann and three-mode theories give more reliable results because the signal with higher frequency propagates faster. With the elementary theory one cannot detect this effect. An important conclusion is also related to the fact that a good damage position indicator may be obtained from the relative distance between the reflections from the crack places and the element end. Then, the differences in wave propagation speed noticed for the theories tested do not affect the general damage detection method. That might be an indication for future work related to creating proper and adequate damage identification criteria based on the differences in propagating waves.

Another important conclusion is that before choosing a proper model, analysis is required of the wavenumbers for a specific material and geometry. When the excitation signal frequency does not excite the higher modes the Love rod theory gives very good results. For excitation signal frequencies which excite higher modes the Mindlin–Herrmann or the three-mode rod theory should be applied.

Acknowledgements

The authors are grateful to the support of the Polish Research Council via KBN Grant no. T07C 007 25 entitled: "*Application of Lamb waves for structural damage detection*". M. Palacz would also thank the Foundation for Polish Science for being granted the Scholarschip for Young Scientists, edition 2003.

References

[1] F.-K. Chang (Ed.), *Structural Health Monitoring: Current Status and Perspectives*, Technomic Publishing Co., Inc., Lancaster, Basel, 1997.
[2] F.-K. Chang (Ed.), *Structural Health Monitoring: Current Status and Perspectives*, Technomic Publishing Co., Inc., Lancaster, Basel, 1999.
[3] F.-K. Chang (Ed.), *Structural Health Monitoring: Current Status and Perspectives*, Technomic Publishing Co., Inc., Lancaster, Basel, 2001.
[4] R.D. Adams, P. Cawley, The Localisation of Defects in Structures from Measurements of Natural Frequencies, *Journal of Strain Analysis* 14 (1979) 49–57.
[5] P. Cawley, R.D. Adams, C.J. Pye, B.J. Stone, A vibration technique for non-destructively assessing the integrity of structures, *Journal of Mechanical Engineering Sciences* 20 (1978) 93–100.
[6] I. Messina, A. Jones, E.J. Williams, Damage detection and localisation using natural frequency changes, in: *Proceedings of the First Conference on Structural Identification*, Cambridge, 1992, pp. 67–76.
[7] M. Krawczuk, W. Ostachowicz, Damage indicators for diagnostic of fatigue cracks in structures by vibration measurements—a survey, *Journal of Theoretical and Applied Mechanics* 34 (1996) 307–326.
[8] T.W. Lim, T.A.L. Kashangaki, Structural damage detection of space truss structures using best achievable eigenvectors, *AIAA Journal* 30 (1994) 2310–2317.
[9] C. Farrar, D. Jauregui, Damage detection algorithms applied to experimental and numerical modal data from I–40 bridge, Report No. LA–13074, Los Alamos National Laboratory, Los Alamos, NM,1996.
[10] K.A. Lakshmanan, D.J. Pines, Modelling damage in composite rotorcraft flexbeams using wave mechanics, *Smart Materials and Structures* 6 (1997) 383–392.
[11] S.A. Rizzi, J.F. Doyle, A Spectral Element Approach to Wave Motion in Layered Solids, *Journal of Vibration and Acoustics* 114 (1992) 569–577.
[12] D.R. Mahapatra, S. Golpalakrishnan, A spectral finite element model for analysis of axial–flexural–shear coupled wave propagation in laminated composite beams, *Computers and Structures* 59 (2003) 67–88.
[13] M. Krawczuk, Application of spectral beam finite element with a crack and iterative search technique for damage detection, *Finite Elements in Analysis and Design* 38 (2002) 537–548.
[14] M. Krawczuk, M. Palacz, W. Ostachowicz, The dynamic analysis of cracked Timoshenko beam by the spectral element method, *Journal of Sound and Vibration* 264 (2003) 1139–1153.
[15] J.F. Doyle, *Wave Propagation in Structures*, Springer, New York, 1997.

[16] M. Palacz, M. Krawczuk, Analysis of longitudinal wave propagation in a cracked rod by the spectral element method, *Computers and Structures* 80 (2002) 1809–1816.
[17] A.D. Dimarogonas, S.A. Paipetis, *Analytical Methods in Rotor Dynamics*, Applied Science Publishers, London, 1983.
[18] H. Tada, P.C. Paris, G.R. Irwin, *The Stress Analysis of Cracks Handbook*, Del Research Corporation, 1973.
[19] M.Krawczuk, J.Grabowska, M.Palacz, Longitudinal wave propagation. Part 1—comparison of rod theories, *Journal of Sound and Vibration* (2006), accepted for publication.